THE GEOLOGICAL SOCIETY OF AMERICA®

An improved approach to age-modeling in deep time: Implications for the Santa Cruz Formation, Argentina

Robin B. Trayler[1,2,†], Mark D. Schmitz[1], José I. Cuitiño[3], Matthew J. Kohn[1], M. Susana Bargo[4], Richard F. Kay[5], Caroline A.E. Strömberg[6], and Sergio F. Vizcaíno[4]

[1]*Department of Geosciences, Boise State University, 1910 University Drive, Boise, Idaho 83725, USA*
[2]*Department of Life and Environmental Sciences, University of California Merced, 5200 Lake Road, Merced, California 95343, USA*
[3]*Instituto Patagónico de Geología y Paleontología, CENPAT-CONICET, Boulevard Almirante Brown 2915, Puerto Madryn, U9120ACD, Chubut, Argentina (CIC and CONICET)*
[4]*División Paleontología de Vertebrados, Museo de La Plata, Unidades de Investigación, Anexo Museo, Av. 60 y 122, 1900, La Plata, Argentina*
[5]*Department of Evolutionary Anthropology, Trinity College and Division of Earth and Ocean Sciences, Nicholas School of the Environment, Duke University, Durham, North Carolina 27708, USA*
[6]*Department of Biology and Burke Museum of Natural History and Culture, University of Washington, Seattle, Washington 98195, USA*

ABSTRACT

Accurate age-depth models for proxy records are crucial for inferring changes to the environment through space and time, yet traditional methods of constructing these models assume unrealistically small age uncertainties and do not account for many geologic complexities. Here we modify an existing Bayesian age-depth model to foster its application for deep time U-Pb and $^{40}Ar/^{39}Ar$ geochronology. More flexible input likelihood functions and use of an adaptive proposal algorithm in the Markov Chain Monte Carlo engine better account for the age variability often observed in magmatic crystal populations, whose dispersion can reflect inheritance, crystal residence times and daughter isotope loss. We illustrate this approach by calculating an age-depth model with a contiguous and realistic uncertainty envelope for the Miocene Santa Cruz Formation (early Miocene; Burdigalian), Argentina. The model is calibrated using new, high-precision isotope dilution U-Pb zircon ages for stratigraphically located interbedded tuffs, whose weighted mean ages range from ca. 16.78 ± 0.03 Ma to 17.62 ± 0.03 Ma. We document how the Bayesian age-depth model objectively reallocates probability across the posterior ages of dated horizons, and thus produces better estimates of relative ages among strata and variations in sedimentation rate. We also present a simple method to propagate age-depth model uncertainties onto stratigraphic proxy data using a Monte Carlo technique. This approach allows us to estimate robust uncertainties on isotope composition through time, important for comparisons of terrestrial systems to other proxy records.

INTRODUCTION

Placing measurements of proxy records (e.g., fossils, geochemical data, pollen or phytolith abundances) in a broader geochronologic context is crucial for inferring environmental and faunal variations in space and time. For proxy records where stratigraphic position is known, chronology construction relies on both accurate and precise age determinations and an age-depth model that describes the relationship between stratigraphic position and time. This process is complicated by the underlying uncertainties in both the age determinations and the complex nature of sediment accumulation. Furthermore, datable materials are often intermittently distributed and are not necessarily co-located with the proxy record of interest, resulting in uncertainty in correlation and interpolation.

Considerable effort has been expended on how best to interpolate time from dated to undated stratigraphic positions, and a variety of proposed statistical methods have been proposed for this purpose (see reviews of: Blaauw and Heegaard, 2012; Parnell et al., 2011). Broadly, these methods can be split into two categories: classical and Bayesian models. Classical age-depth modeling encompasses a variety of deterministic linear, spline, and polynomial interpolation methods that aim to fit a smooth curve that relates stratigraphic position to age. The resulting models do not necessarily pass through each measured age, instead they are fit as closely as possible to each point, usually by a least squares approach (Blaauw and Heegaard, 2012). With the addition of Monte Carlo methods to simulate the underlying uncertainties in age, probabilistic classical models may produce satisfactory chronologies. However, they have several limitations. First, classical models do not explicitly consider stratigraphic relationships among samples and may produce chronologies that violate superposition and imply negative accumulation rates (See fig. 6 in Blaauw and Heegaard, 2012). Second, these methods often underestimate the uncertainties associated with undated positions (Blaauw et al., 2018; De Vleeschouwer and Parnell, 2014).

Bayesian inference offers an alternative to the classical approach by combining data (age determinations) and prior information (stratigraphic positions) to generate a satisfactory probabilistic posterior chronology. Originally developed for radiocarbon calibration and chronology construction (Blaauw and Christen, 2005; Bronk Ramsey, 2008; Haslett and Parnell, 2008), Bayesian age-depth modeling has become increasingly applied to other types of geochronologic data (De Vleeschouwer and Parnell, 2014; Sahy et al., 2015; Wotzlaw et al., 2018).

In this paper we introduce a modified version of an existing Bayesian age-depth model, Bchron (Haslett and Parnell, 2008), for use with U-Pb, $^{40}Ar/^{39}Ar$, and other deep time geochronologic data. We then illustrate our approach for the Miocene (Burdigalian) Santa Cruz Formation of southern Argentina (Fig. 1). We use our new dates, cast within a Bayesian framework, as a test case to address two broad questions. First, how

[†]rtrayler@ucmerced.edu

GSA Bulletin; https://doi.org/10.1130/B35203.1; 7 figures; 3 tables; Data Repository item 2019241.

does the inclusion of prior information affect the interpretation of the non-symmetric uncertainties that arise from the analysis of several individual mineral grains (e.g., zircon, sanidine)? Second, how can the significant uncertainties associated with age-depth models be considered in the interpretations of proxy records?

BAYESIAN MODELING

Bayesian models attempt to estimate the probable values of unknown *parameters* based on *prior* information about these parameters, which can be conditioned by observed data, or *likelihoods*. The relationship between these terms is formalized in Bayes' theorem:

$$P(\theta \mid x) \propto \frac{P(x \mid \theta)}{P(x)} \times P(\theta). \qquad (1)$$

The first term on the right-hand side of Equation 1 is the conditional probability of the data given the proposed parameters, i.e., how probable are our data (x; age determinations) given a proposed parameter (θ; model age). The second term is the probability associated with any prior knowledge of the parameters (θ), i.e., for our example, how constraints such as stratigraphic superposition and/or assumptions of sedimentation rate and its variability affect the probability of the proposed age parameters (θ). The left-hand term is the posterior conditional probability of the proposed parameters, i.e., what is the most probable age (θ) given how our data (i.e., the radiometric age determinations) and our prior knowledge (stratigraphic position, sedimentation rate variability) interact.

In most cases Bayes' theorem cannot be solved analytically, so we instead generate a representative sample of the posterior distribution using Markov Chain Monte Carlo (MCMC) methods. MCMC uses a variety of probabilistic proposal algorithms to produce a random sample of the posterior distribution. Given a large enough sample size and adequate exploration of parameter space, this sample should be representative of the "true" posterior distribution and should have the same underlying summary statistics (Kruschke, 2015).

Bayesian Age-Depth Modeling with Bchron

Originally designed for radiocarbon calibration and age-depth modeling, Bchron is available as an open source R package (Haslett and Parnell, 2008). Bchron generates an age model, given specific age determinations, associated uncertainties, and stratigraphic positions. The model treats sedimentation as a series of accumulation events of varying duration and amount, where the number of accumulation events is drawn from a Poisson distribution and the amount of accumulation is drawn from a gamma distribution. These two processes are related using a compound Poisson-gamma distribution to describe the *prior* probability of the sedimentation events (Haslett and Parnell, 2008). In addition to the parameters associated with age determinations, Bchron uses two hyperparameters (μ, ψ) to control the mean and dispersion of the compound Poisson-gamma distribution. Because these hyperparameters (μ, ψ) are calculated over the entire section, accumulation paths that have roughly the same mean accumulation rate are effectively favored. This method results in a model that is piecewise linear and allows for a wide variety of possible accumulation paths (Fig. 2).

A piecewise linear process is desirable for several reasons. First, the process is monotonically increasing such that stratigraphically higher positions are always younger than those below, thus capturing the fundamental stratigraphic principle of superposition. Second, the process allows for a wide range of sedimentation paths and there is no a priori assumption of smoothly varying sedimentation rates. While classical methods often assume that accumulation rates vary only at dated positions or vary smoothly in between, a piecewise linear process with a varying number of change points allows for segments that imply near-zero (disconformity-like) to very rapid accumulation rates (Haslett and Parnell, 2008). Confidence intervals of chronologies based on classical methods often exhibit a waist or hourglass effect where model uncertainties counterintuitively decrease as distance from dated positions increases, underestimating uncertainty at these positions (De Vleeschouwer and Parnell, 2014; Telford et al., 2004). Conversely, by allowing the number of sedimentation events to vary by both duration and amount, Bchron model probabilities are presented as a highest density interval (HDI), which is similar to a confidence interval but makes no prior assumptions about the distribution shape. These HDI's take on a sausage-like shape where uncertainty increases with distance from dated positions. This phenomenon captures the expectation that uncertainty should increase in areas poorly constrained by data.

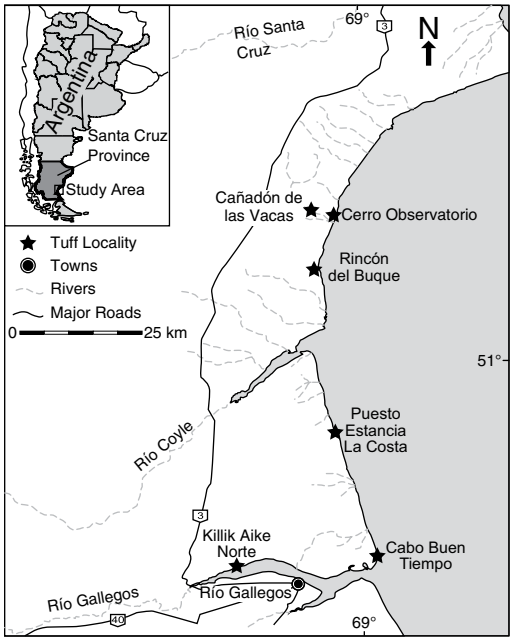

Figure 1. Map of tuff localities, Santa Cruz Formation, Argentina.

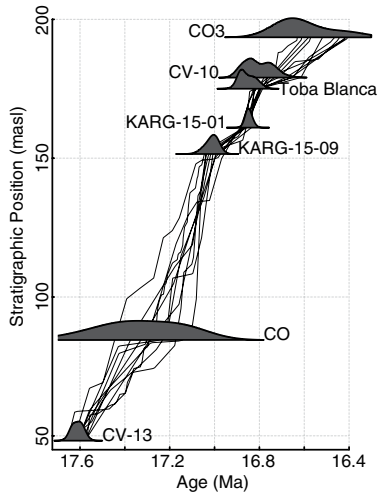

Figure 2. Ten example chronologies, Santa Cruz Formation, Argentina. Note that a wide variety of chronologies are possible in the lower section, while the upper section where ash beds are more closely spaced requires tightly bunched model paths. CO—Cerro Observatorio; CV—Cañadón de las Vacas; masl—meters above sea level.

GEOLOGIC SETTING OF SANTA CRUZ FORMATION SAMPLES

We focus on the Santa Cruz Formation because it is one of the most fossiliferous sedimentary sequences in South America and provides an unparalleled opportunity to link paleoclimate and faunal evolution immediately prior to the mid-Miocene climatic optimum (Vizcaíno et al., 2012b). The formation is part of the Miocene infill of the South American Austral Basin. It trends NW-SE, is bounded by the Patagonian

Andes in the west and the Deseado Massif in the northeast and is open to the Atlantic Ocean toward the east and southeast. During the Miocene, Andean uplift and crustal loading drove an increase in accommodation space, allowing the accumulation of the terrestrial deposits of the Santa Cruz Formation (Blisniuk et al., 2005; Bown and Fleagle, 1993; Cuitiño et al., 2019; Fosdick et al., 2013; Marshall, 1976). Outcrops of these Santa Cruz Formation deposits are extensive, with exposures from the Andean foothills to the Atlantic coast (Blisniuk et al., 2005; Cuitiño and Scasso, 2010; Fleagle et al., 2012; Malumián et al., 1999; Marshall, 1976; Tauber, 1994, 1997). While geographically widespread, the exposures are discontinuous, and depositional idiosyncrasies make some sections less amenable to dating. However, because such large areas of the Santa Cruz Formation are exposed, age controls from multiple localities can be integrated using lithological and tephrochronological correlations (see fig. 2.2 in Perkins et al., 2012).

There has been considerable effort to constrain the age of the Santa Cruz Formation and its fossil localities. K-Ar dates placed the Santa Cruz Formation in the late-early to middle Miocene (Evernden et al., 1964; Marshall et al., 1977) and at 16–17 Ma (Marshall et al., 1986). $^{40}Ar/^{39}Ar$ analyses for coastal exposures included a range from ca. 19.3 to ca. 16.2 Ma (Fleagle et al., 1995) and an age of 16.68 ± 0.11 Ma for a tuff from the Killik Aike Norte locality (Tejedor et al., 2006). Dates from western exposures ranged from 22.4 to 14.2 Ma (Blisniuk et al., 2005). To synthesize these ages, Perkins et al. (2012) and Fleagle et al. (2012) reported new $^{40}Ar/^{39}Ar$ ages for several tuffs, recalibrated previous dates, correlated tuffs (and their ages) across many Santa Cruz Formation localities using tephrochronology and constructed a chronostratigraphic framework for much of the Santa Cruz Formation. More recently Cuitiño et al. (2016) reported four U-Pb ages from strata exposed along the Río Bote and Río Santa Cruz, allowing correlation from western to eastern exposures.

TABLE 1. GPS COORDINATES AND ELEVATION, COMPOSITE STRATIGRAPHIC POSITION, AND WEIGHTED MEAN AGES FOR ALL SAMPLES FROM THE SANTA CRUZ FORMATION, ARGENTINA

Sample	Locality	Latitude	Longitude	GPS elevation (m)	Stratigraphic position (masl)	Weighted mean age (Ma)
CV-10	CV	–50.55754	–69.15467	195	179	16.825 ± 0.036
Toba Blanca	CV	–50.5572	–69.15482	185	175	16.868 ± 0.032
KARG-15-01	CV	–50.5646	–69.15071	181	161	16.850 ± 0.022
KARG-15-09	CV	–50.6550	–69.21211	96	84.5 ± 2.5	17.006 ± 0.039
CV-13	CO	–50.6016	–69.08627	-	48.25 ± 3.13	17.615 ± 0.026
KAN1	KAN	–51.5747	–69.44655	4.9	-	16.996 ± 0.025
KARG-15-08	CBT	–51.52684	–68.95529	41	-	16.949 ± 0.030
KARG-15-12	PLC	–51.19278	–68.89952	105	-	16.783 ± 0.051

Notes: CV—Cañadón de las Vacas; CO—Cerro Observatorio; KAN—Killik Aike Norte; CBT—Cabo Buen Tiempo; PLC—Puesto Estancia la Costa; masl—meters above sea level.

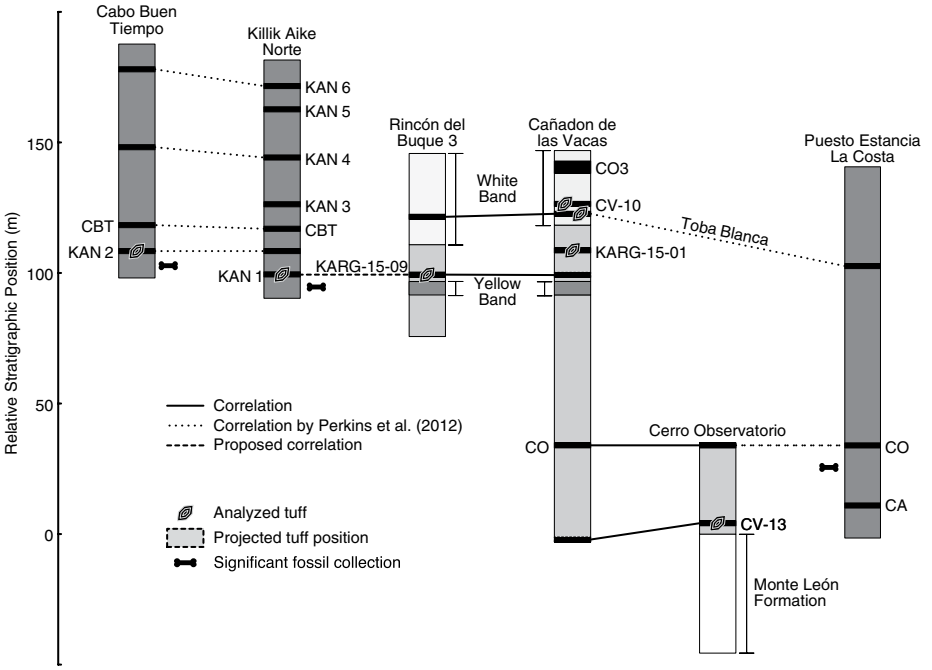

Figure 3. Correlation diagram for Santa Cruz Formation, Argentina, localities considered in this study. The geographic location of each locality is shown in Figure 1. Colored stratigraphic columns are used to form the composite section shown in Figure 5. Stratigraphic columns for Cabo Buen Tiempo (CBT), Killik Aike Norte (KAN), and Puesto Estancia La Costa modified from Perkins et al. (2012). CO—Cerro Observatorio; CV—Cañadón de las Vacas; CA—Corriguen Aike.

MATERIALS AND METHODS

U-Pb Geochronology

We analyzed tuffs from six Santa Cruz Formation localities: Cañadón de las Vacas, Rincón del Buque 3, Cerro Observatorio, Killik Aike Norte, Cabo Buen Tiempo, and Puesto Estancia La Costa (Fig. 1; Table 1). Combined with the stratigraphic framework of Perkins et al. (2012), our new mapping and stratigraphic sections allow correlations among these sites (Fig. 3). We follow the abbreviations of Perkins et al. (2012) for locality and tuff names whenever possible to facilitate comparisons of our ages with theirs.

All mineral separations and isotope analyses took place in the Boise State Isotope Geology Laboratory, Boise, Idaho, USA. Zircon crystals were separated from each sample using density and magnetic methods. The resulting crystal concentrates were heated in a muffle furnace at 900 °C for 60 h to anneal minor radiation damage and prepare crystals for chemical abrasion. After annealing, individual grains were hand-picked, mounted in epoxy, polished to their centers using silicon carbide lapping film and 0.3 µm alumina, and imaged by cathodoluminescence (CL).

After imaging, we analyzed 30–40 crystals from each sample via laser ablation–inductively coupled plasma–mass spectrometry (LA-ICP-MS) using a ThermoElectron X-Series II quadrupole ICP-MS and a New Wave Research UP-213 Nd:YAG UV (213 nm) laser ablation system. Details of the LA-ICP-MS methodology are reported in Macdonald et al. (2018). LA-ICP-MS $^{206}Pb/^{238}U$, dates, U content, CL zoning pattern, and visual clarity were then used to select single zircon grains for chemical abrasion–isotope dilution–thermal ionization mass spectrometry (CA-ID-TIMS) analysis. Individual crystals were chemically abraded in concentrated hydrofluoric acid at 180 °C for 12 h to remove mineral

inclusions and mitigate open system behavior (Mattinson, 2005). Residual crystals were then spiked with the ET535 isotope dilution tracer (Condon et al., 2015; McLean et al., 2015) and processed for chemical abrasion isotope dilution thermal ionization mass spectrometry (CA-ID-TIMS; Macdonald et al., 2018). Isotope ratios were measured using an IsotopX Phoenix X62 or Isoprobe-T mass spectrometer; U-Pb dates and uncertainties were calculated using the methods of Schmitz and Schoene (2007) and the U decay constants of Jaffey et al. (1971). Errors for calculated weighted means are reported in the form ± X(Y)[Z] where X is the analytical uncertainty, Y is the combined analytical and tracer (EARTHTIME 535; Condon et al., 2015; McLean et al., 2015) uncertainties, and Z is the combined analytical, tracer, and decay constant uncertainties. Repeated measurements of the EARTHTIME ET100 U-Pb isotope ratio standard solution are reported in Table DR5[1], and document no significant overdispersion relative to the propagated uncertainties of the analyses, while demonstrating agreement with the long-term average values measured in the Boise State University Isotope Geology Laboratory.

Model Modifications

In this study we modified the Bchron compound Poisson-gamma age-depth model for use with U-Pb and $^{40}Ar/^{39}Ar$ data in deep time stratigraphic contexts. Our model is implemented as an R package (R Core Team, 2019), available for download at https://github.com/robintrayler/modifiedBChron. Here we outline our modifications.

Assignment of Age Uncertainties

We allow individual dates to be grouped to form complex probability density functions, reproducing the practice in both U-Pb and $^{40}Ar/^{39}Ar$ geochronology of convolving many single crystal or spot analyses into a single age model. Modern high precision dates on single mineral crystals from volcanic rocks often demonstrate dispersion beyond analytical uncertainty (Jicha et al., 2016; Rivera et al., 2013). Consequently, the resulting age probability estimation for each dated horizon is a complex function that can be modeled as a summed probability density plot or kernel density estimate (Vermeesch, 2012), which we will generically call a "probability distribution." We have included the ability to combine individual dates based on a grouping variable (e.g., from the same stratigraphic horizon). Within each group, individual dates and uncertainties are specified by the user as either normal (or uniform) distributions, and then summed within the algorithm on the basis of the grouping variable to form the final probability distributions for each dated horizon. By grouping data in this way, the user can model arbitrarily complex radioisotopic age, magnetic reversal, or even detrital zircon maximum depositional age likelihood distributions.

Markov Chain Monte Carlo Implementation

We implement an adaptive Markov Chain Monte Carlo algorithm to remove the need for data rescaling. Bchron and our model use a Metropolis-Hastings algorithm to evaluate Bayes' equation and produce a posterior sample for each model parameter. Briefly, for each iteration of each Markov chain a new parameter is proposed from a Gaussian proposal distribution centered on the current parameter value. The proposed parameter and current parameter are compared and accepted or rejected probabilistically (Brooks et al., 2011; Chib and Greenberg, 1995; Kruschke, 2015). In effect the algorithm randomly walks through the parameter space. The efficiency of this algorithm depends heavily on an appropriately scaled proposal distribution. However, without a priori information about the target distribution, selecting an appropriately scaled proposal distribution is difficult. Bchron addresses this problem by rescaling the input data (age determinations, age uncertainties, stratigraphic positions) to limit the possible size of the proposal distribution. While the restricted time and spatial scales of radiocarbon chronologies are amenable to this approach, it is inflexible for deeper time data that may be presented in thousands (ka), millions (Ma), or billions (Ga) of years as they require vastly different scaling factors. A variety of adaptive proposal algorithms have been developed to address this problem (e.g., Christen and Fox, 2010; Gelman et al., 1996; Haario et al., 2001; Roberts and Rosenthal, 2009). Here we use the adaptive proposal algorithm of Haario et al. (1999) to ensure that the parameter space (i.e., the set of all possible values for a parameter) is efficiently explored. In this method the proposal distribution for each dated horizon is defined as:

$$\theta_i = N(\theta_{i-1}, c_d^2 \sigma_h^2), \quad (2)$$

where θ_{i-1} is the current model age in the Markov Chain for a specific horizon, θ_i is the proposed model age at the same horizon, σ_h^2 is the variance of the previous h iterations in the Markov Chain, and c_d is an empirically determined constant scaling factor. We use $c_d = 2.4$ as recommended by Gelman et al. (1996) and Haario et al. (1999). In effect, the variance of each model parameter is monitored during each simulation and a unique proposal distribution for each parameter is adjusted accordingly.

Outlier Rejection

We have removed automated outlier rejection. Instead we prescreen our data for outliers using a variety of established criteria based on the physical mechanisms of crystal growth and open system behavior in volcanic rocks. Biased dates for mineral crystals primarily arise from three processes. First, open system behavior resulting from the loss of radiogenic daughter isotopes biases analyses to apparently younger ages. Second, mineral inclusions within a crystal may have anomalous daughter to parent isotope ratios and/or initial daughter contents, which contaminate and bias the resulting dates to apparently older ages. Finally, inheritance or recycling of geologically older crystals produces dates that are older than the eruptive age of the target magmatic event. A variety of analytical methods have been developed to minimize these systematic outliers for U-Pb and $^{40}Ar/^{39}Ar$ data. For zircon crystals, chemical abrasion prior to analysis reduces the influence of open system behavior and contamination by selectively removing inclusions and damaged portions of the zircon lattice most susceptible to loss of radiogenic lead (Mattinson, 2005). When lead loss is intransigent, even after chemical abrasion, its effect may be identified and those samples manually excluded, through comparisons of covariance of $^{206}Pb/^{238}U$ and $^{207}Pb/^{235}U$ (Wetherill, 1956, 1963). Likewise, the development of the step heating method for $^{40}Ar/^{39}Ar$, coupled with careful examination of the resulting age spectrum for argon-bearing minerals using a plot of cumulative ^{39}Ar versus age and the inverse isochron diagram allow open system behavior in these systems to be monitored (McDougall and Harrison, 1999).

For both dating systems, crystal recycling or inheritance, either from much older country rock (xenocrysts) or slightly older volcanic materials from the same volcanic system (antecrysts) may produce dates older than the actual time of eruption. Xenocrysts that are significantly older than the dominant age mode are trivial to reject. In some cases, slightly older antecrysts may be removed by the application of several statistical rejection criteria (Michel et al., 2016), although these effects are often subtle. We focus here on the ability of Bayesian age modeling to objectively mitigate these antecryst effects by quantitatively rejecting older age modes using superpositional constraints.

[1]GSA Data Repository item 2019241, Figures DR1–DR4; Appendix 1, example code; and Tables DR1–DR5, is available at http://www.geosociety.org/datarepository/2019 or by request to editing@geosociety.org.

RESULTS

U-Pb CA-ID-TIMS

Summary location and age information for each sample are listed in Table 1, while the full data acquired by LA-ICP-MS (Tables DR3 and DR4) and CA-ID-TIMS (Table DR5) are reported in the supplementary material.

Killik Aike Norte (KAN)

Killik Aike Norte (KAN; 51° 34′ S, 69° 25′ W) is a series of exposures along the north banks of the Río Gallegos estuary, located ~100 km south of Cerro Observatorio along the Atlantic coast. The Santa Cruz Formation is exposed in the walls of a deep canyon that enters the river channel from the north, with continuous exposures along the northern banks of the river itself (Marshall, 1976). Tejedor et al. (2006) illustrated a stratigraphic column and reported an $^{40}Ar/^{39}Ar$ age of 16.68 ± 0.05 Ma (recalibrated by Perkins et al., 2012) for a vitric tuff from KAN. However, analysis of a pumice clast within the tephra gives an $^{40}Ar/^{39}Ar$ age of 17.06 ± 0.07 Ma (Perkins et al., 2012). We collected a new sample of the KAN tuff for analysis to address this discrepancy.

KAN-1

CL imaging of zircon from the KAN-1 tuff revealed predominantly equant, oscillatory zoned crystals. A minority of grains exhibited an elongate, prismatic morphology but were otherwise similar to the equant population. CL-dark inherited cores were common and avoided. Of 39 grains analyzed by LA-ICP-MS, 24 grains (61%) returned Miocene $^{206}Pb/^{238}U$ ages (Table DR4). Of these grains, fourteen grains were selected for CA-ID-TIMS analysis on the basis of CL zoning patterns and LA-ICP-MS $^{206}Pb/^{238}U$ date. Of these, four analyses had a radiogenic to common lead ratio <1 and were discarded. Of the remaining crystals, six analyses were concordant, of equivalent age, and returned a weighted mean $^{206}Pb/^{238}U$ date of 16.996 ± 0.014(0.017)[0.025] Ma (mean square weighted deviation (MSWD) = 2.51; n = 6), which is interpreted as estimating the eruption age of the tuff (Fig. 4). Five older analyses were assumed to represent either reworked detritus or an older period of zircon growth, and were excluded from the weighted mean calculation.

Cerro Observatorio (CO) and Cañadón De Las Vacas (CV)

Cerro Observatorio (previously known as Monte Observación; 50° 36′ S, 69° 05′ W) is a series of exposures along the Atlantic coast. Cerro Observatorio outcrops at the Atlantic coast. Historically Cerro Observatorio has been synonymized with the Cañadón de las Vacas locality (50° 34′ S, 69° 09′ W) which is located ~6 km NW of the coastal exposures. In this study we consider Cerro Observatorio to refer only to the coastal exposures and refer to the slightly inland exposures as Cañadón de las Vacas. Together, these localities are the richest and most studied of the Santa Cruz Formation, and have produced thousands of fossils (Bown and Fleagle, 1993; Fleagle et al., 2012; Vizcaíno et al., 2012a). We collected three tuffs for analysis from CV (CV-10, KARG-15-01, Toba Blanca), and one from CO (CV-13). Perkins et al. (2012) dated or recalibrated ages of several tuffs from these localities. With the exception of the Toba Blanca, which we reanalyzed, we chose undated tuffs for analysis.

KARG-15-01

CL imaging of zircon from the KARG-15-01 tuff revealed a uniform population of prismatic, oscillatory zoned crystals. A minority of grains contained CL distinct rounded cores that were avoided in all subsequent analyses. Of 38 grains analyzed by LA-ICP-MS, 37 grains (97%) returned Miocene $^{206}Pb/^{238}U$ ages (Table DR4). Five grains were selected for CA-ID-TIMS analysis on the basis of LA-ICP-MS $^{206}Pb/^{238}U$ date and CL zoning. These analyses were concordant, of indistinguishable isotope ratios, and returned a weighted mean $^{206}Pb/^{238}U$ date of 16.850 ± 0.009(0.013)[0.022] Ma (MSWD = 0.43; n = 5), which is interpreted as estimating the eruption age of the tuff.

CV-10

CL imaging of zircon from the CV-10 tuff revealed a uniform population of weakly zoned, elongate prismatic crystals. Inherited cores and large inclusions were rare and avoided. Of 21 grains analyzed by LA-ICP-MS, 10 grains (48%) returned Miocene $^{206}Pb/^{238}U$ ages (Table DR4). Eleven grains were selected for CA-ID-TIMS analysis. Five analyses had a radiogenic to common lead ratio of <1 and were discarded. Two grains yielded $^{206}Pb/^{238}U$ dates >19 Ma and were set aside as inheritance. The remaining four grains are concordant and have indistinguishable isotope ratios with a weighted mean $^{206}Pb/^{238}U$ date of 16.825 ± 0.030(0.031)[0.036] Ma (MSWD = 3.17; n = 4), which is interpreted as estimating the eruption age.

Toba Blanca

CL imaging of zircon from the Toba Blanca revealed a mixed population of weakly zoned, equant to elongate prismatic crystals. Large mineral inclusions were common and were avoided. Of 30 grains analyzed by LA-ICP-MS, 25 grains (83%) returned Miocene $^{206}Pb/^{238}U$ ages (<23.03 Ma; Table DR4). Ten grains were selected for CA-ID-TIMS analysis. Five analyses had a radiogenic to common lead ratio <1 and were discarded. An additional grain yielded a $^{206}Pb/^{238}U$ date of >23 Ma and was set aside as inherited. Of the four remaining grains, three are concordant and have indistinguishable isotope ratios, with a weighted mean $^{206}Pb/^{238}U$ date of 16.868 ± 0.025(0.026)[0.032] Ma (MSWD = 1.82; n = 3), which is interpreted as estimating the eruption age. A single grain with a $^{206}Pb/^{238}U$ date ca. 0.15 Ma older than the weighted mean was also excluded as detrital or inherited.

CV-13

CL imaging of zircon from the CV-13 tuff revealed a uniform population of elongate, prismatic, oscillatory zoned crystals. CL dark inherited cores were common and avoided. Of 30 grains analyzed by LA-ICP-MS, 21 grains (70%) returned Miocene $^{206}Pb/^{238}U$ ages (Table DR4). Sixteen grains were selected for CA-ID-TIMS analysis. Two analyses had a radiogenic to common lead ratio <1 and were discarded. Four additional grains with $^{206}Pb/^{238}U$ dates >19 Ma were also set aside as inherited detritus. Five of the nine remaining grains yielded concordant and indistinguishable isotope ratios with a weighted mean $^{206}Pb/^{238}U$ date of 17.620 ± 0.015(0.017)[0.026] Ma (MSWD = 1.44; n = 5), which is interpreted as the eruption age of the tuff. Four slightly older grains were excluded from the weighted mean calculation and are assumed to represent either detrital or pre-eruptive grains.

Cabo Buen Tiempo (CBT)

At Cabo Buen Tiempo (51° 34′ S, 68° 57′ W), Santa Cruz Formation strata (including fossiliferous levels and numerous tuffs) are exposed on a tidal platform at low tide and in an adjacent sea cliff. Perkins et al. (2012) correlated several CBT tuffs to other localities. The only direct date of a CBT tuff is imprecise (<17.73 Ma; Perkins et al., 2012). We collected a sample of the lowest exposed tuff (~41 m above sea level) at Cabo Buen Tiempo (KARG-15-08). Based on the stratigraphic scheme of Perkins et al. (2012), this is likely the KAN-2 tuff.

KAN-2

CL imaging of zircon from the KARG-15-08 tuff revealed a mixed population of elongate and equant, prismatic, oscillatory zoned crystals. Inherited cores were uncommon and avoided. Of 37 grains analyzed by LA-ICP-MS, 31 grains (84%) returned Miocene $^{206}Pb/^{238}U$ ages (Table DR4). Nineteen grains were selected for CA-ID-TIMS analysis. Six analyses had a radiogenic to com-

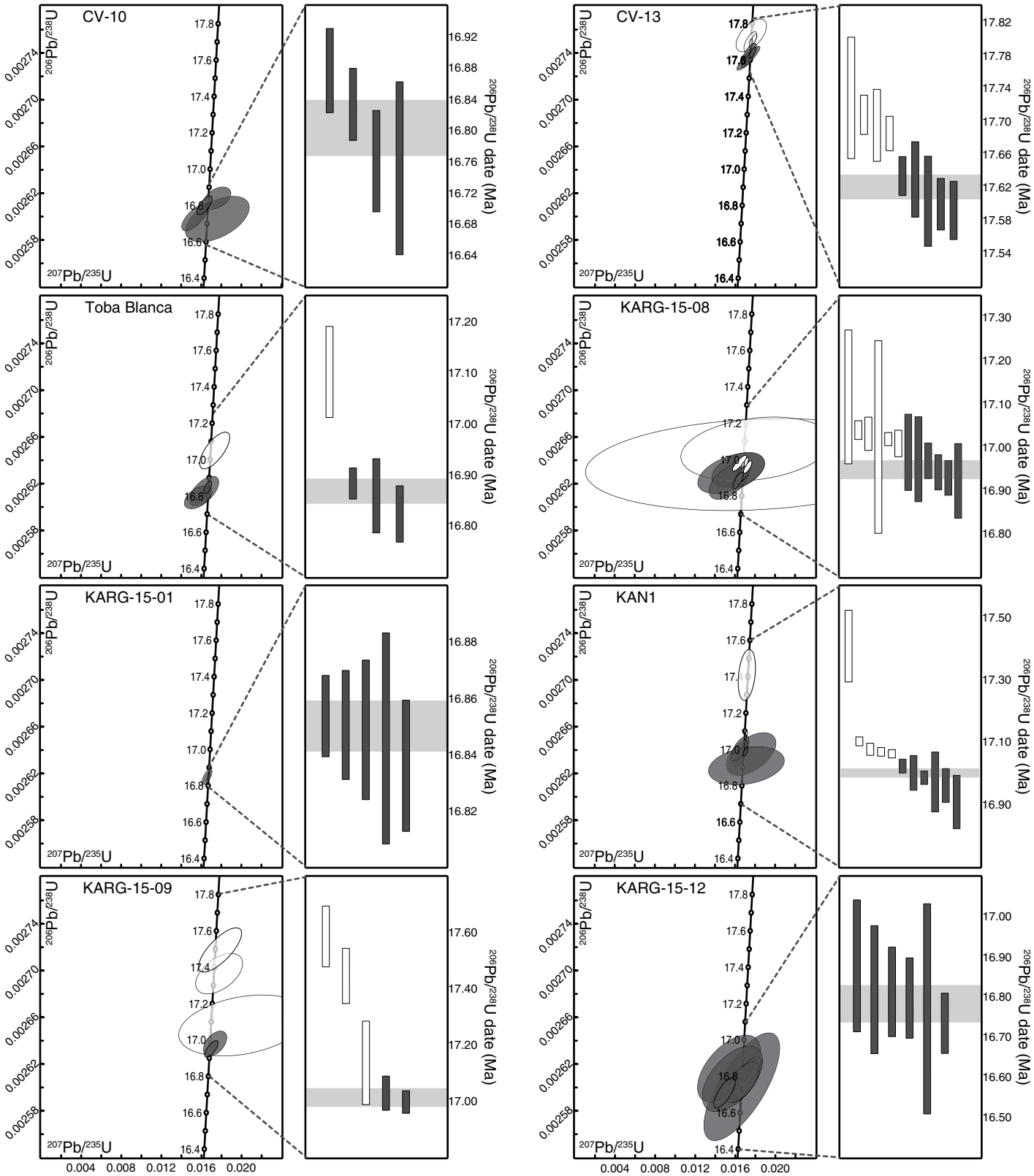

Figure 4. U-Pb Concordia and ranked age plots for all analyzed samples, Santa Cruz Formation, Argentina. Shaded symbols indicate analyses included in weighted mean calculations. The light gray band on ranked age plots indicates the weighted mean. All uncertainties are shown as 2σ. CV—Cañadón de las Vacas; KAN—Killik Aike Norte.

mon lead ratio <1 and were rejected. An additional grain with a $^{206}Pb/^{238}U$ date of >19 Ma was also rejected as probable inheritance. Of the remaining twelve grains the six youngest grains are concordant and of indistinguishable isotope ratio, with a weighted mean $^{206}Pb/^{238}U$ date of 16.949 ± 0.022(0.023)[0.030] Ma (MSWD = 0.68; n = 6), which is interpreted as estimating the eruption age. Four slightly older grains were excluded from the weighted mean calculation and are assumed to represent either inheritance or an earlier period of zircon growth. Two other grains with very high $^{206}Pb/^{238}U$ date uncertainties ($2\sigma > 0.15$ Ma) were also excluded.

Rincón Del Buque (RB)

Located ~10 km S-SE of Cerro Observatorio and Cañadón de las Vacas, Rincón del Buque (50° 39′ S, 69° 12′ W) is a large half-moon shaped amphitheater (Marshall, 1976; Raigemborn et al., 2015; Vizcaíno et al., 2012a) exposing the Santa Cruz Formation as a series of benches and cliffs. We collected a single tuff (KARG-15-09) for analysis from Rincón del Buque 3 (RB3). This locality outcrops along the north of the Rincón Del Buque amphitheater at the border between Estancias Cañadón de las Vacas and Ototel Aike, Argentina.

KARG-15-09

CL imaging of zircon from the KARG-15-09 tuff revealed a mixture of equant and elongate, prismatic, oscillatory zoned crystals. Inherited cores and large inclusions were common and avoided. Of 34 grains analyzed by LA-ICP-MS, 17 grains (50%) returned Miocene $^{206}Pb/^{238}U$ ages (Table DR4). Seventeen grains were selected for CA-ID-TIMS analysis. Eleven analyses had a radiogenic to common lead ratio of <1 and were discarded. One analysis yielded a Cretaceous date of ca. 106 Ma and was discarded. Of the remaining five grains, two grains are concordant, of indistinguishable isotope ratio with a weighted mean $^{206}Pb/^{238}U$ date of 17.006 ± 0.034(0.035) [0.039] Ma (MSWD = 1.83; n = 2), which is interpreted as estimating the eruption age. A single grain with a high (>0.1 Ma) uncertainty was excluded from the weighted mean calculation. Two ca. 0.3–0.4 Ma older grains were also excluded from the weighted mean calculation and are assumed to be detrital or inherited.

Puesto Estancia La Costa (PLC)

Puesto Estancia La Costa (51° 11′ S, 69° 05′ W) is the most productive fossil locality of the Santa Cruz Formation (Fleagle et al., 2012; Vizcaíno et al., 2012a), with the Santa Cruz Formation exposures partially below sea level except at low tide, leading to constant tidal excavation of new material. The locality has produced numerous complete skeletons and some of the southernmost examples of primate fossils (Vizcaíno et al., 2010; 2012a). We collected a single tuff (KARG-15-12) exposed near the top of the section.

KARG-15-12

CL imaging of zircon from the KARG-15-12 tuff revealed a mixed population of equant to elongate, prismatic, oscillatory zoned crystals. Inherited cores and large inclusions are uncommon and were avoided. Of 33 grains analyzed by LA-ICP-MS, 24 grains (72%) returned Miocene $^{206}Pb/^{238}U$ ages (Table DR4). Eight grains were selected for CA-ID-TIMS analysis. One grain had a radiogenic to common lead ratio of <1 and was discarded. Another grain with a $^{206}Pb/^{238}U$ date >18 Ma was set aside as inherited or detrital. The remaining seven grains are concordant and have indistinguishable isotope ratios, with a weighted $^{206}Pb/^{238}U$ date of 16.783 ± 0.047(0.048) [0.051] Ma (MSWD = 0.72; n = 6).

Model Validation

The goal of MCMC algorithms is to produce a posterior sample that is stable, representative, and reproducible (Kruschke, 2015). The underlying compound Poisson-gamma process of Bchron has been repeatedly validated. Using synthetic data, Haslett and Parnell (2008) showed that ~80–95% of model highest density intervals (HDIs) encompass the "true" accumulation path. Parnell et al. (2011) compared several Bayesian age-depth models, including Bchron, using three metrics; modal distance, proportion of contained probability distributions, and the Kullback-Leiber divergence measure. Briefly, modal distance is the difference between the mode of a model posterior distribution and the mode of the input likelihoods. Kullback-Leiber divergence is similar to modal distance except that it compares the entire probability distribution instead of summary statistics (i.e., modes). Both modal distance and Kullback-Leiber divergence calculations suggest that Bchron does not diverge unnecessarily from the points where age is best understood. The proportions of contained probability distributions are calculated using a leave-one-out cross validation, where individual age determinations are excluded from a data set. The resulting model is then compared to the excluded age. Parnell et al. (2011) showed that ~50% of excluded ages were completely contained within model 95% HDIs.

Our modified model uses the same underlying statistical framework as Bchron and repeated comparisons revealed only small differences between Bchron and our modified version, which are comparable to those observed among individual Bchron runs (Fig. DR1; see footnote 1). We therefore focused on examining the performance of our model across repeated model runs to ensure that our modifications do not affect model stability.

To assess model performance, we generated 500 individual simulations for the Santa Cruz Formation data set. Each simulation comprised 10,000 iterations with the initial 5000 steps discarded to allow the model to stabilize (i.e., burn-in). First, we examined the trajectory of each model parameter using trace plots (Fig. DR2; see footnote 1). Individual trace plots for each parameter stabilized quickly and mixed well. Comparing all 500 model simulations showed no visual difference between model runs for each parameter. Similarly, probability density estimates (kernel density estimates) of each model parameter were visually indistinguishable between simulations (Fig. DR3; see footnote 1). We also monitored variability in the lower bounds, upper bounds, and median of the 95% HDI across all model runs. The median was stable and varied only slightly (±0.004 Ma; 2σ). The lower and upper bounds of the HDI also show little change among iterations (±0.006 Ma; 2σ).

Modeling the Santa Cruz Formation

We developed two age-depth models for the Santa Cruz Formation, based on a composite stratigraphy of the CV locality, one using weighted mean ages, and another using the summed probability distributions of all analytically acceptable dates as inputs. For each model we included dates from CV (KARG-15-01, CV-10, Toba Blanca), and those from the nearby RB3 (KARG-15-09) and CO (CV-13) localities. The stratigraphic positions of these tuffs were projected into the CV composite by proportionally scaling the distance between marker beds of known stratigraphic position at each locality (Fig. 3). We also include $^{40}Ar/^{39}Ar$ ages for two tuffs at Cañadón de las Vacas (CO, CO3) previously reported by Perkins et al. (2012).

When weighted mean ages were used as the data likelihood for each tuff (Fig. 5A), the median for each posterior age likelihood distribution differed from the input weighted mean ages by only a few thousand years (Table 2). In the upper section, where there is considerable overlap between weighted mean ages, median model ages were consistently younger (Fig. 6), as a consequence of the superpositional model prior. Perhaps more importantly, posterior age uncertainties for each tuff were also reduced compared to weighted means by 10–20% (0.01–0.04 Ma), reflecting the positive effects of each dated horizon on those nearby.

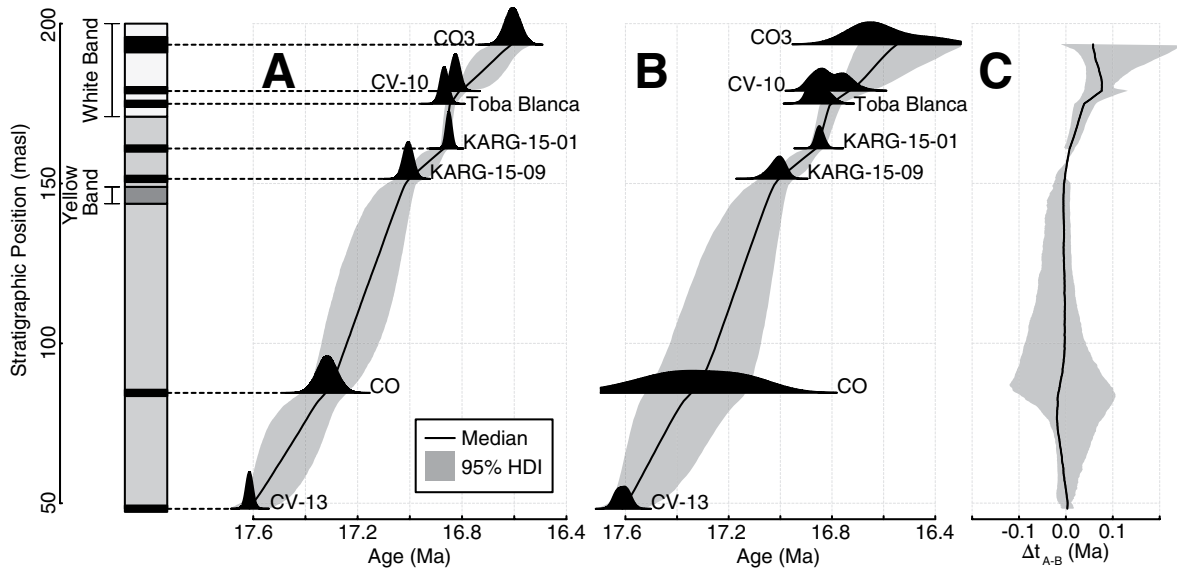

Figure 5. Age models and simplified stratigraphic column for the composite of the Cañadón de las Vacas-Cerro Observatorio-Rincón de Buque section, Santa Cruz Formation, Argentina. Shaded probability distributions are the specified likelihood distribution for each tuff. The 95% highest density interval (HDI) (light gray shading) indicates the model uncertainty for all interpolated points between tuffs, while the black line indicates the median. (A) Model results using weighted mean ages as likelihood inputs. (B) Model results using the summed probability distribution function for each tuff as likelihood input. (C) Difference between the two models. As expected, model uncertainties are higher in B because of the increased variance of the specified likelihoods. The difference in the model median is close to zero in the lower section, while in the upper section, B is shifted toward younger ages. CO—Cerro Observatorio; CV—Cañadón de las Vacas; masl—meters above sea level.

TABLE 2. SUMMARY STATISTICS OF THE LIKELIHOOD AND POSTERIOR AGE FOR EACH TUFF FROM THE COMPOSITE CAÑADÓN DE LAS VACAS SECTION, SANTA CRUZ FORMATION, ARGENTINA

Sample	Locality	Weighted mean likelihood		Summed probability distribution likelihood	
		Weighted mean (Ma)	95% HDI model age (Ma)	95% HDI (Ma)	95% HDI model age (Ma)
†*CO3	CO	16.61 ± 0.060	16.61 + 0.06/–0.06	16.62 + 0.21/–0.32	16.55 + 0.15/–0.26
*CV-10	CV	16.825 ± 0.036	16.809 + 0.023/–0.030	16.812 + 0.102/–0.136	16.732 + 0.057/–0.080
*Toba Blanca	CV	16.868 ± 0.032	16.845 + 0.017/–0.020	16.860 + 0.060/–0.082	16.806 + 0.039/–0.045
*KARG-15-01	CV	16.850 ± 0.022	16.867 + 0.017/–0.019	16.848 + 0.031/–0.035	16.859 + 0.031/–0.029
*KARG-15-09	RB3	17.006 ± 0.039	17.004 + 0.037/–0.034	17.010 + 0.071/–0.053	17.007 + 0.061/–0.049
†*CO	CO	17.31 ± 0.08	17.32 + 0.07/–0.07	17.32 + 0.41/–0.36	17.34 + 0.18/–0.20
†*CV-13	CO	17.615 ± 0.026	17.616 + 0.026/–0.026	17.612 + 0.053/–0.053	17.613 + 0.055/–0.053

Notes: CV—Cañadón de las Vacas; CO—Cerro Observatorio; RB3—Rincón del Buque 3.

*Weighted mean age uncertainties are reported as a mean ±2σ; all other ages are reported as a median and 95% highest density interval (HDI).

†Weighted mean ages and summed probability distributions recalculated from data for individual $^{40}Ar/^{39}Ar$ laser fusion analyses from Perkins et al. (2012) provided by Matthew Heizler at the New Mexico Geochronological Research Laboratory, Socorro, New Mexico, USA (personal communication, 2018).

When we used the summed probability distribution as the likelihood input (Fig. 5B), the model results showed several differences compared to the weighted mean model. Median model ages were consistently shifted younger when compared to the median of the likelihood probability distribution. Once again, this effect was most common in the upper section where likelihood probability distributions overlap significantly. The magnitude of the shift is also greater with a maximum shift of 0.08 Ma for the CO3 tuff. Model uncertainties for each tuff were also reduced compared to the likelihood probability distribution. The magnitude of reduction in uncertainty was significant, with decreases of up to 40%–50% (0.2–0.4 Ma) for some tuffs (CO, CV-10).

In both models, the model bounds (HDI's) were broadest in the area between the CV-13 and KARG-15-09 tuffs and were much larger than the HDI's of the tuffs. In the upper section where tuffs are more closely spaced, model HDI's were significantly smaller and similar to those of the tuffs themselves. Both the weighted mean model and summed probability distribution model showed the value of collecting high precision dates from closely spaced horizons.

We also investigated the sensitivity of the model to the inclusion of antecrysts (unshaded symbols in Fig. 4) that were otherwise excluded as outliers from our final data set. We generated an age-depth model using all dates for CV-13, CO, KARG-15-09, KARG-15-01, Toba Blanca, CV-10, and CO3. The antecryst model is broadly similar to the final summed probability distribution model (Fig. DR4; see footnote 1) with an average difference between the two of 0.02 Ma for the median and, 0.006 Ma and 0.04 Ma for the lower and upper bounds of the 95% HDI, respectively. The largest difference between the antecryst model and the final summed probability distribution model are in the lower part of the section and are likely attributable to the visibly older mode for sample CV-13. As this sample is the stratigraphically lowest, superpositional constraints cannot reject these older dates. It should be noted, however, that these antecrysts are easily rejected using the methods discussed above. The inclusion of all antecrysts into a single model ultimately represents a worst-case scenario where there was no prescreening of data for outliers.

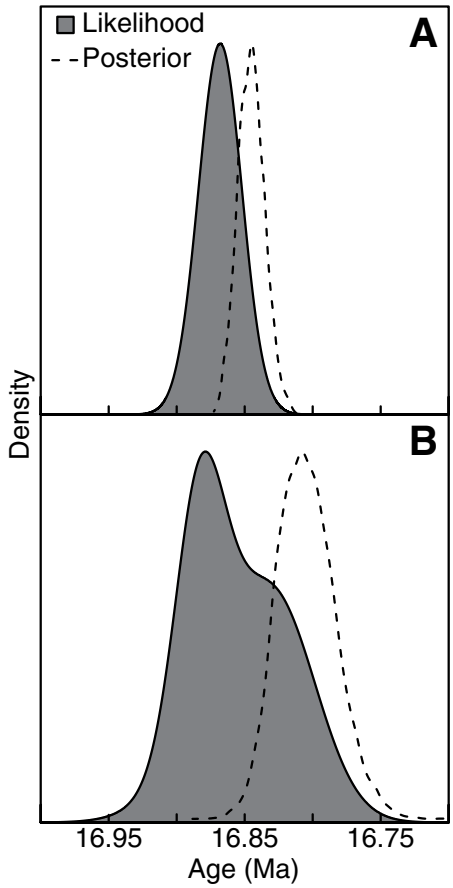

Figure 6. Comparison between the likelihood (shaded area) and posterior (dashed line) probability distribution functions for the Toba Blanca, Santa Cruz Formation, Argentina. (A) Weighted mean likelihood function. (B) Summed probability distribution likelihood function. While both the posterior distribution for both models is shifted toward younger ages, the effect is more pronounced in B. Zircon populations often show prolonged periods of crystallization, with only the youngest populations accurately representing the eruptive age.

The inclusion of any single outlier date into the model has a much less pronounced effect.

DISCUSSION

Bayesian Conditioning of Radioisotopic Ages

Interpreting the eruptive age of volcanic rocks has traditionally focused on careful examination of individual samples, without quantitative consideration of stratigraphic relationships. Similarly, the focus of age-depth modeling is usually to predict the age of points in between dated horizons (De Vleeschouwer and Parnell, 2014; Wotzlaw et al., 2018), while the effect of the model on the input dates themselves is not usually explored. Our results show the value of a hybrid approach, using traditional methods to screen grain dates for obvious outliers arising from diverse physical behaviors (inheritance, daughter isotope loss), while employing a Bayesian framework to condition the remaining dates into eruptive ages that are consistent with superpositional constraints and incorporate the variance seen in many magmatic mineral populations. The value of exploring the model's effect on the input ages themselves is particularly evident in the upper portion of the composite section, where there is considerable overlap between the summed probability distributions of the closely spaced KARG-15-01, Toba Blanca, CV-10, and CO3 tuffs. In particular, the Toba Blanca (Fig. 6), CV-10, and CO3 tuffs have distinct younger modes that the Bchron algorithm favors over higher probability, older modes. In the lower section (KARG-15-09 and below), the less precise $^{40}Ar/^{39}Ar$ dates for the CO tuff exhibits considerable overlap of its probability distribution with both the CV-13 (below) and KARG-15-09 (above) tuffs. Here again the influence of a superposition constraint is evident as the overlapping portions of the CO probability distribution are ignored by the model, reducing the HDI on the CO tuff by ~50%.

Alternatively, using weighted mean ages as a likelihood input produces an age model with lower overall uncertainties for interpolated points. It also results in slightly more rapid accumulation rates in the upper section, while accumulation rates in the lower section are nearly unchanged. Since the likelihood probability distributions are modeled as symmetrical Gaussian distributions, the three upper-most tuffs lack the younger high probability "tails" present in the summed probability distribution model. Consequently, the shift of posterior distributions for each of these tuffs toward younger ages is less pronounced than in the summed probability distribution model.

Accurately modeling an eruptive age in volcanic tuffs is complicated by physical processes of inheritance, crystal recycling, and prolonged periods of crystal growth in magma chambers, which often result in crystal populations with asymmetric probability distributions that may have distinctly younger or older tails (e.g., Toba Blanca, CV-10, CO3 tuffs). This dispersion is best captured using a summed probability model, but does lead to ambiguous cases where the dominant mode is older than the youngest grains. By allowing the consideration of stratigraphic relationships between samples, Bayesian age modeling identifies the younger, lower probability grains as the most probable eruptive age (Figs. 5C and 6). Conversely, some samples (KARG-15-01) are tightly grouped around an expectation value (mean) with no obvious structure to their probability distributions suggesting younger or older modes. In these cases, using weighted mean likelihoods results in overall improved model uncertainties. In principle, using weighted means as model inputs will likely result in higher "precision" results. However, weighted means of either whole crystal populations or a subset, are themselves a model of eruption age, which may or may not be appropriate given the structure of the data (Keller et al., 2018). In cases where the dispersion of crystal populations cannot be attributed solely to analytical uncertainty and in the absence of stratigraphic information, Bayesian methods still offer a useful alternative to determining eruptive age (Keller et al., 2018). Age-depth modeling offers a complementary and alternative approach to interpreting overdispersed crystal populations. Ultimately, the choice of either weighted means or summed probability distributions as likelihoods should be heavily influenced by the structure of the data.

Using Age-Depth Models to Fine-Tune Ages

While model results suggest that the ages of several tuffs require slight adjustments, overall our U-Pb ages and modeled posterior ages are consistent with previous radioisotopic ages for the Santa Cruz Formation. However, our data also include ages for five previously unanalyzed tuffs, which allows the refinement of correlations between localities.

The Toba Blanca is exposed in several coastal exposures of the Santa Cruz Formation (Tauber, 1994), and is distributed laterally over at least 500 km (Perkins et al., 2012), making it an important marker bed for the Santa Cruz Formation. Our weighted mean age for the Toba Blanca (16.868 ± 0.032 Ma) is within uncertainty of an $^{40}Ar/^{39}Ar$ age of 16.89 ± 0.05 Ma, previously published by Perkins et al. (2012). However, our age model results suggest that the Toba Blanca is slightly younger, with an age range of ca. 16.80–16.84 Ma (Fig. 6) that is within uncertainty of both the weighted mean and the HDI of the summed probability distribution for the individual crystal ages. Likewise, model results indicate that both the CV-10 and CO3 tuffs are somewhat younger than their weighted mean ages. In all three cases their probability distributions have distinct younger tails, suggesting that the older modes do not represent the eruptive age and instead record a prolonged period of crystal growth or recycling from earlier magmatism. These complications present the question, what are the "correct" ages for these tuffs? In our view, given the observed dispersion in individual zircon ages, and the stratigraphic superposition relationship with a less complex tuff (i.e., KARG-15-01), the modeled posterior ages for the summed prob-

ability distributions (Table 2) are the most robust and realistic eruptive ages.

Implications for Correlations within the Santa Cruz Formation

Our data permit new correlations between the Cañadón de las Vacas composite section and other analyzed Santa Cruz Formation localities (Fig. 3). The weighted mean ages of the KAN-1 (Killik Aike Norte) and KARG-15-09 (Rincón del Buque 3) tuffs are statistically indistinguishable and we therefore propose these coeval tuffs represent a single eruptive event. Given that the Rincón del Buque 3 and Killik Aike Norte are separated by ~100 km, a new correlative tuff over this distance provides a valuable marker bed between the two localities. The sample KARG-15-08 (16.949 ± 0.030 Ma; CBT) was collected from the lowest exposed tuff at CBT and was previously identified as the KAN-2 tuff. The age of the tuff was inferred by Perkins et al. (2012) as ca. 16.9 Ma, which is supported by our results. Given that the KAN-2 tuff is also exposed ~5 m above the KAN-1 tuff at Killik Aike Norte (Perkins et al., 2012; Tejedor et al., 2006), our results add a new age constraint for this locality.

Using Age Models to Interpret Proxy Records

Exposures of the Santa Cruz Formation at Lago Posadas (~47° 60′ S, 71° 51′ W) preserve at least 500 m of stratigraphic section. Blisniuk et al. (2005) proposed an age range of ca. 22–14 Ma, but reevaluation of the section by Perkins et al. (2012), Cuitiño et al. (2015, 2019) imply that the base of the Santa Cruz Formation is at ca. 19 Ma. Blisniuk et al. (2005) reported $^{40}Ar/^{39}Ar$ ages for six tuffs and stable carbon ($\delta^{13}C$) isotope ratios of ~250 paleosol carbonate nodules from Lago Posadas. Paleosol nodules are uniformly distributed throughout the section (0–39 m between samples) and are not co-located with dated tuffs. We used our modified modeling approach discussed above to generate a new age-model for the Lago Posadas section, and developed a simple method for propagating the significant uncertainties associated with age model outputs onto the paleoclimate proxy. We used weighted mean ages for the upper five tuffs as model inputs. We excluded the stratigraphically lowest age reported by Blisniuk et al. (2005), as Perkins et al. (2012) noted that this tuff (LP-10) was "unsuitable for an age," and regional correlations indicate a younger age at this level (Cuitiño et al., 2015, 2019; Perkins et al., 2012).

Using our model (Fig. 7A; Table 3), we estimated the age and its uncertainty for each carbonate nodule based on its stratigraphic position. These uncertainties are large, typically >±1 Ma. Given that changes in isotope composition are commonly used as a proxy for ecological, climatological, and tectonic change (Koch, 1998; Poage and Chamberlain, 2001), it is extremely important to incorporate these significant age uncertainties during the transformation from the spatial (stratigraphic height) domain to the time series, and the subsequent analysis and correlation of these isotopic records to global change (Blaauw et al., 2007; Parnell et al., 2008).

Discrete stratigraphic proxy record samples (e.g., stable isotopes, palynofloras, phytolith assemblages) are commonly transformed into a continuous temporal record through the use of age models and smoothing and interpolation functions. Many age-depth transformations are deterministic in nature, while most common smoothing functions (moving averages, polynomials, splines) assume that errors are either nonexistent or normally distributed. Both of these assumptions are inconsistent with our models' prediction of age for each proxy record (carbonate nodules). Each age-depth model consists of many possible sample chronologies (e.g., Fig. 2). By using these probabilistic chronologies to predict the age of the carbonate nodules, the age of each nodule is allowed to vary while still preserving the superpositional relationships among nodules. This is accomplished using the following steps:

(1) Use age-depths model results to choose a set of ages for each proxy record based on its stratigraphic position.

(2) Apply an appropriate smoothing function (in this case a moving average) to the proxy data (in this case carbon isotopes) given the chosen set of ages and store the results.

(3) Repeat many times and calculate summary statistics (e.g., median, HDI) over all smoothed proxy records.

A moving average through the Lago Posadas carbon isotope data (from Blisniuk et al. 2005) versus stratigraphic position (Fig. 7B) illustrates the limitations of fitting a single smoothing function to a data set. In stratigraphic regions with low data density (e.g., ~200 and 290 m), the single moving average model shows significant spikes and wiggles in isotope composition. These abrupt variations include a rapid increase at 200–215 m that Blisniuk et al. (2005) interpreted as beginning at ca. 16.5 Ma based upon a deterministic age model. The authors attributed this shift to an increase aridity driven by a pulse of Andean uplift at 16.5 Ma. However, when age model uncertainties are considered it becomes clear that where there is low data density in a *stratigraphic* context, there are many other samples of similar overlapping *ages* (Fig. 7C), which must influence and reallocate the probability of the proxy value in the temporal domain. While the single moving average model suggests rapid shifts in $\delta^{13}C$ in the stratigraphic reference frame, propagated age model uncertainties instead suggest that in a rigorous probabilistic temporal reference frame, $\delta^{13}C$ values possibly began increasing ~0.6 m.y. earlier at 17.1 Ma, and continued gradually until at least 16 Ma, with $\delta^{13}C$ values then remaining essentially unchanged until the end of the record.

The use of a probabilistic age-depth model and the propagation of model uncertainties therefore has implications for both the timing and rate of isotopic change. The moving average model originally reported by Blisniuk et al. (2005) implies that the initial increase in $\delta^{13}C$ values at 200–215 m could have occurred rapidly over as little as ~0.06 m.y., whereas our re-evaluation permits a much more gradual increase extending over ~1 m.y. Significantly, an increase in $\delta^{13}C$ values at the revised age of ca. 17 Ma corresponds to the onset of the mid-Miocene climatic optimum, a period of overall increased global temperatures (Holbourn et al., 2015; Zachos et al., 2001). Global climate change may therefore provide a plausible alternative explanation for the vegetation shifts that drove changes to $\delta^{13}C$ values. Finally, converting stratigraphic position to age also simplifies and lends rigor to comparisons of proxy records between localities that lack correlative stratigraphic features. This stratigraphic to temporal transformation is vital for terrestrial sequences sensitive to hiatuses and rapid changes in depositional environment and rate.

CONCLUSIONS

While Bayesian age-depth modeling is commonly used with Quaternary radiocarbon ages, existing models have seen only limited deep-time use. We have demonstrated the features of a modified Bayesian age-depth model amenable to deep time scenarios using new U-Pb ages of zircon and existing $^{40}Ar/^{39}Ar$ ages from the Santa Cruz Formation. Proposed tuff correlations link exposures at Killik Aike Norte to the upper section at Cañadón de las Vacas and Rincón de Buque, providing a new correlation among these localities.

We view our model results as largely consistent with both our U-Pb and existing $^{40}Ar/^{39}Ar$ data for the Santa Cruz Formation, requiring only small adjustments to ages. While these shifts are small, we view model results as the most robust estimate of age. In many cases the model improves uncertainties of imprecise data (i.e., CO, CO3 tuffs). The greatest improvements occur when closely spaced tuffs are dated, further showing the value of dating several samples through a stratigraphic section. Allowing the model to explore the full variance present in magmatic zircon

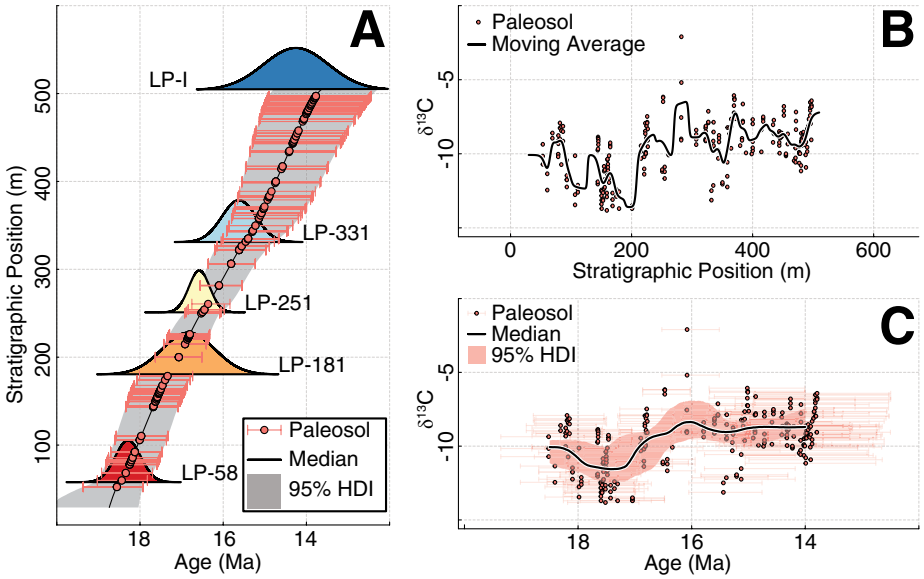

Figure 7. (A) Age-depth model for Lago Posadas, Argentina. Pink points and error bars indicate the median and 95% HDI model ages for paleosol carbonate nodules. (B) Plot of the carbon isotope composition of paleosol carbonates versus stratigraphic position, with a weighted moving average with a 5 m window size. (C) Plot of carbonate carbon isotope compositions versus age. Error bars indicate the 95% high density interval (HDI) of age for each point as in A. Black line is the median of 100,000 Gaussian weighted moving averages (0.2 Ma window size), where the age of each point was allowed to vary probabilistically based on age model results. Ninety-five percent of the moving average models fall within the shaded pink area.

TABLE 3. SUMMARY STATISTICS OF THE LIKELIHOOD AND POSTERIOR AGE FOR EACH TUFF FROM THE LAGO POSADAS SECTION, SANTA CRUZ FORMATION, ARGENTINA

Sample	Stratigraphic position (m)	Weighted mean likelihood	
		Weighted mean (Ma)	95% HDI model age (Ma)
LP-I	504.5	14.24 ± 1.56	13.64 + 1.14/–1.35
LP-331	331.5	15.61 ± 0.82	15.46 + 0.59/–0.68
LP-251	251.7	16.56 ± 0.50	16.49 + 0.39/–0.45
LP-181	181.2	16.82 ± 1.62	17.29 + 0.67/–0.61
LP-58	58.8	18.27 ± 0.62	18.45 + 0.59/–0.60

Notes: Weighted mean ages uncertainties are reported as a mean ±2σ; all other ages are reported as a median and 95% highest density interval (HDI). Weighted mean ages were originally reported in Blisniuk et al. (2005) and recalibrated by Perkins et al. (2012).

populations offers an outlier rejection method that quantitatively incorporates superposition.

Translating proxy records from the *stratigraphic reference frame* to time requires a robust Bayesian age model and its propagation of model uncertainties. While the high frequency structure in the Lago Posadas paleosol record could for example arise from cyclic climatic forcing, it could also plausibly be an artifact of changes in sedimentation rate. A variety of tools exist to address the former scenario (Meyers, 2015, 2019) if it is warranted by strong evidence. In the second case, using model uncertainties to inform the interpretation of proxy record data also shows promise. Reanalysis of carbon isotope data from the Lago Posadas paleosol record (Blisniuk et al. 2005) with age model uncertainty reveals a gradual increase in $\delta^{13}C$ values from ca. 17–16 Ma, suggesting the probability of both an earlier initiation and slower change than originally reported. We view this as a more conservative and robust interpretation of the proxy record, which highlights the general need (Blaauw et al., 2018) for the collection of stratigraphically dense, high-precision geochronologic data cast within a robust Bayesian age model framework.

ACKNOWLEDGMENTS

We thank Dr. James Crowley for his assistance with LA-ICP-MS and CA-ID-TIMS analyses and Dr. Jacob Anderson for assistance with model development. We also thank two anonymous reviewers for their helpful feedback and suggestions, which led to an improved final manuscript. This work was funded by National Science Foundation grants EAR-1349749 (MJK), EAR-1349741 (RFK), and EAR-1349530 (CAES). Funding for the analytical infrastructure of the Boise State Isotope Geology Laboratory was provided by the National Science Foundation (EAR-0521221, EAR-0824974, EAR-1337887, EAR-1735889).

REFERENCES CITED

Blaauw, M., and Christen, J.A., 2005, Radiocarbon peat chronologies and environmental change: Journal of the Royal Statistical Society. Series C, Applied Statistics, v. 54, no. 4, p. 805–816, https://doi.org/10.1111/j.1467-9876.2005.00516.x.

Blaauw, M., and Heegaard, E., 2012, Estimation of age-depth relationships, *in* Birks, H., Lotter, A., Juggins, S., and Smol, J., eds., Tracking Environmental Change Using Lake Sediments. Developments in Paleoenvironmental Research: Dordrecht, The Netherlands, Springer, v. 5, p. 379–413, https://doi.org/10.1007/978-94-007-2745-8_12.

Blaauw, M., Christen, J., Mauquoy, D., van der Plicht, J., and Bennett, K., 2007, Testing the timing of radiocarbon-dated events between proxy archives: The Holocene, v. 17, no. 2, p. 283–288, https://doi.org/10.1177/0959683607075857.

Blaauw, M., Christen, J.A., Bennett, K., and Reimer, P.J., 2018, Double the dates and go for Bayes: Impacts of model choice, dating density and quality on chronologies: Quaternary Science Reviews, v. 188, p. 58–66, https://doi.org/10.1016/j.quascirev.2018.03.032.

Blisniuk, P.M., Stern, L.A., Chamberlain, C.P., Idleman, B., and Zeitler, P.K., 2005, Climatic and ecologic changes during Miocene surface uplift in the Southern Patagonian Andes: Earth and Planetary Science Letters, v. 230, no. 1, p. 125–142, https://doi.org/10.1016/j.epsl.2004.11.015.

Bown, T.M., and Fleagle, J.G., 1993, Systematics, biostratigraphy, and dental evolution of the Palaeothentidae, later Oligocene to early–middle Miocene (Deseadan–Santacrucian) caenolestoid marsupials of South America: Journal of Paleontology, v. 67, no. S29, p. 1–76.

Bronk Ramsey, C., 2008, Deposition Models For Chronological Records: Quaternary Science Reviews, v. 27, no. 1, p. 42–60, https://doi.org/10.1016/j.quascirev.2007.01.019.

Brooks, S., Gelman, A., Jones, G., and Meng, X.-L., 2011, Handbook of Markov Chain Monte Carlo: New York, USA, Chapman and Hall, 619 p., https://doi.org/10.1201/b10905.

Chib, S., and Greenberg, E., 1995, Understanding the Metropolis-Hastings algorithm: The American Statistician, v. 49, no. 4, p. 327–335.

Christen, J.A., and Fox, C., 2010, A general purpose sampling algorithm for continuous distributions (the t-walk): Bayesian Analysis, v. 5, no. 2, p. 263–281, https://doi.org/10.1214/10-BA603.

Condon, D., Schoene, B., McLean, N., Bowring, S., and Parrish, R., 2015, Metrology and traceability of U-Pb isotope dilution geochronology (EARTHTIME Tracer Calibration Part I): Geochimica et Cosmochimica Acta, v. 164, p. 464–480, https://doi.org/10.1016/j.gca.2015.05.026.

Cuitiño, J.I., and Scasso, R.A., 2010, Sedimentología y paleoambientes del Patagoniano y su transición a la Formación Santa Cruz al sur del Lago Argentino, Patagonia Austral: Revista de la Asociación Geológica Argentina, v. 66, no. 3, p. 406–417.

Cuitiño, J.I., Ventura Santos, R., Alonso Muruaga, P.J., and Scasso, R.A., 2015, Sr-stratigraphy and sedimentary evolution of early Miocene marine foreland deposits in the northern Austral (Magallanes) Basin, Argentina: Andean Geology, v. 42, no. 3, p. 364–385.

Cuitiño, J.I., Fernicola, J.C., Kohn, M.J., Trayler, R.B., Naipauer, M., Bargo, M.S., Kay, R.F., and Vizcaíno, S.F., 2016, U-Pb geochronology of the Santa Cruz Formation (early Miocene) at the Río Bote and Río Santa Cruz (southernmost Patagonia, Argentina): Implications for the correlation of fossil vertebrate localities: Journal of South American Earth Sciences, v. 70, p. 198–210, https://doi.org/10.1016/j.jsames.2016.05.007.

Cuitiño, J.I., Vizcaíno, S.F., Bargo, M.S., and Aramendía, I., 2019, Sedimentology and fossil vertebrates of the Santa Cruz Formation (early Miocene) in Lago Posadas, southwestern Patagonia, Argentina: Andean Geology (in press).

De Vleeschouwer, D., and Parnell, A.C., 2014, Reducing time-scale uncertainty for the Devonian by integrating

astrochronology and Bayesian statistics: Geology, v. 42, no. 6, p. 491–494, https://doi.org/10.1130/G35618.1.

Evernden, J., Savage, D., Curtis, G., and James, G., 1964, Potassium-argon dates and the Cenozoic mammalian chronology of North America: American Journal of Science, v. 262, no. 2, p. 145–198, https://doi.org/10.2475/ajs.262.2.145.

Fleagle, J.G., Bown, T., Swisher, C., and Buckley, G., 1995, Age of the Pinturas and Santa Cruz formations: Proceedings Congreso Argentino de Paleontología y Bioestratigrafía, p. 129–135.

Fleagle, J.G., Perkins, M.E., Heizler, M.T., Nash, B., Bown, T.M., Tauber, A.A., Dozo, M.T., and Tejedor, M.F., 2012, Absolute and relative ages of fossil localities in the Santa Cruz and Pinturas Formations, *in* Vizcaíno, S.F., Kay, R.F., and Bargo, M.S., eds., Early Miocene Paleobiology in Patagonia: High-Latitude Paleocommunities of the Santa Cruz Formation: Cambridge, UK, Cambridge University Press, p. 41–58, https://doi.org/10.1017/CBO9780511667381.004.

Fosdick, J.C., Grove, M., Hourigan, J.K., and Calderon, M., 2013, Retroarc deformation and exhumation near the end of the Andes, southern Patagonia: Earth and Planetary Science Letters, v. 361, p. 504–517, https://doi.org/10.1016/j.epsl.2012.12.007.

Gelman, A., Roberts, G.O., and Gilks, W.R., 1996, Efficient Metropolis jumping rules: Bayesian Statistics, v. 5, p. 599–607.

Haario, H., Saksman, E., and Tamminen, J., 1999, Adaptive proposal distribution for random walk Metropolis algorithm: Computational Statistics, v. 14, no. 3, p. 375–396, https://doi.org/10.1007/s001800050022.

Haario, H., Saksman, E., and Tamminen, J., 2001, An adaptive Metropolis algorithm: Bernoulli, v. 7, no. 2, p. 223–242, https://doi.org/10.2307/3318737.

Haslett, J., and Parnell, A.C., 2008, A simple monotone process with application to radiocarbon-dated depth chronologies: Applied Statistics, v. 57, no. 4, p. 399–418.

Holbourn, A., Kuhnt, W., Kochhann, K.G., Andersen, N., and Meier, K.S., 2015, Global perturbation of the carbon cycle at the onset of the Miocene Climatic Optimum: Geology, v. 43, no. 2, p. 123–126, https://doi.org/10.1130/G36317.1.

Jaffey, A., Flynn, K., Glendenin, L., Bentley, W.t., and Essling, A., 1971, Precision measurement of half-lives and specific activities of U^{235} and U^{238}: Physical Review C: Nuclear Physics, v. 4, no. 5, https://doi.org/10.1103/PhysRevC.4.1889.

Jicha, B.R., Singer, B.S., and Sobol, P., 2016, Re-evaluation of the ages of $^{40}Ar/^{39}Ar$ sanidine standards and supereruptions in the western U.S. using a Noblesse multi-collector mass spectrometer: Chemical Geology, v. 431, p. 54–66, https://doi.org/10.1016/j.chemgeo.2016.03.024.

Keller, C.B., Schoene, B., and Samperton, K.M., 2018, A stochastic sampling approach to zircon eruption age interpretation: Geochemical Perspectives Letters, v. 8, https://doi.org/10.7185/geochemlet.1826.

Koch, P.L., 1998, Isotopic reconstruction of past continental environments: Annual Review of Earth and Planetary Sciences, v. 26, no. 1, p. 573–613, https://doi.org/10.1146/annurev.earth.26.1.573.

Kruschke, J., 2015, Doing Bayesian Data Analysis: A Tutorial With R, JAGS, and Stan: Cambridge, Massachusetts, USA, Academic Press.

Macdonald, F.A., Schmitz, M.D., Strauss, J.V., Halverson, G.P., Gibson, T.M., Eyster, A., Cox, G., Mamrol, P., and Crowley, J.L., 2018, Cryogenian of Yukon: Precambrian Research, v. 319, p. 114–143, https://doi.org/10.1016/j.precamres.2017.08.015.

Malumián, N., Ardolino, A., Franchi, M., Remesal, M., and Salani, F., 1999, La sedimentación y el volcanismo terciarios en la Patagonia extraandina, *in* Proceedings Geología Argentina. Instituto de Geología y Recursos Minerales: Anales, v. 29, p. 557–612.

Marshall, L.G., 1976, Fossil localities for Santacrucian (early Miocene) mammals, Santa Cruz Province, southern Patagonia, Argentina: Journal of Paleontology, v. 50, no. 6, p. 1129–1142.

Marshall, L.G., Pascual, R., Curtis, G.H., and Drake, R.E., 1977, South American geochronology: Radiometric time scale for middle to late Tertiary mammal-bearing horizons in Patagonia: Science, v. 195, no. 4284, p. 1325–1328, https://doi.org/10.1126/science.195.4284.1325.

Marshall, L.G., Drake, R.E., Curtis, G.H., Butler, R.F., Flanagan, K.M., and Naeser, C.W., 1986, Geochronology of type Santacrucian (middle Tertiary) land mammal age, Patagonia, Argentina: The Journal of Geology, v. 94, no. 4, p. 449–457, https://doi.org/10.1086/629050.

Mattinson, J.M., 2005, Zircon U-Pb chemical abrasion ("CA-TIMS") method: Combined annealing and multi-step partial dissolution analysis for improved precision and accuracy of zircon ages: Chemical Geology, v. 220, no. 1, p. 47–66, https://doi.org/10.1016/j.chemgeo.2005.03.011.

McDougall, I., and Harrison, T.M., 1999, Geochronology and Thermochronology by the $^{40}Ar/^{39}Ar$ Method: Oxford, UK, Oxford University Press.

McLean, N.M., Condon, D.J., Schoene, B., and Bowring, S.A., 2015, Evaluating uncertainties in the calibration of isotopic reference materials and multi-element isotopic tracers (EARTHTIME Tracer Calibration Part II): Geochimica et Cosmochimica Acta, v. 164, p. 481–501, https://doi.org/10.1016/j.gca.2015.02.040.

Meyers, S.R., 2015, The evaluation of eccentricity-related amplitude modulation and bundling in paleoclimate data: An inverse approach for astrochronologic testing and time scale optimization: Paleoceanography, v. 30, no. 12, p. 1625–1640, https://doi.org/10.1002/2015PA002850.

Meyers, S.R., 2019, Cyclostratigraphy and the problem of astrochronologic testing: Earth-Science Reviews, v. 190, p. 190–223, https://doi.org/10.1016/j.earscirev.2018.11.015.

Michel, L.A., Schmitz, M.D., Tabor, N.J., Moontañez, I.P., and Davydov, V.I., 2016, Reply to the comment on "Chronostratigraphy and paleoclimatology of the Lodève Basin, France: Evidence for a pan-tropical aridification event across the Carboniferous–Permian boundary" by Michel et al., (2015). Palaeogeography, Palaeoclimatology, Palaeoecology 430, 118–131: Palaeogeography, Palaeoclimatology, Palaeoecology, v. 441, p. 1000–1004, https://doi.org/10.1016/j.palaeo.2015.10.023.

Parnell, A.C., Haslett, J., Allen, J.R., Buck, C.E., and Huntley, B., 2008, A flexible approach to assessing synchroneity of past events using Bayesian reconstructions of sedimentation history: Quaternary Science Reviews, v. 27, no. 19, p. 1872–1885, https://doi.org/10.1016/j.quascirev.2008.07.009.

Parnell, A.C., Buck, C.E., and Doan, T.K., 2011, A review of statistical chronology models for high-resolution, proxy-based Holocene palaeoenvironmental reconstruction: Quaternary Science Reviews, v. 30, no. 21, p. 2948–2960, https://doi.org/10.1016/j.quascirev.2011.07.024.

Perkins, M.E., Fleagle, J.G., Heizler, M.T., Nash, B., Bown, T., Tauber, A., and Dozo, M., 2012, Tephrochronology of the Miocene Santa Cruz and Pinturas Formations, Argentina, *in* Vizcaíno, S.F., Kay, R.F., and Bargo, M.S., eds., Early Miocene Paleobiology in Patagonia: High-Latitude Paleocommunities of the Santa Cruz Formation, p. 23–40, https://doi.org/10.1017/CBO9780511667381.003.

Poage, M.A., and Chamberlain, C.P., 2001, Empirical relationships between elevation and the stable isotope composition of precipitation and surface waters: Considerations for studies of paleoelevation change: American Journal of Science, v. 301, no. 1, p. 1–15, https://doi.org/10.2475/ajs.301.1.1.

Raigemborn, M.S., Matheos, S.D., Krapovickas, V., Vizcaíno, S.F., Bargo, M.S., Kay, R.F., Fernicola, J.C., and Zapata, L., 2015, Paleoenvironmental reconstruction of the coastal Monte Léon and Santa Cruz formations (Early Miocene) at Rincón del Buque, Southern Patagonia: A revisited locality: Journal of South American Earth Sciences, v. 60, p. 31–55, https://doi.org/10.1016/j.jsames.2015.03.001.

R Core Team, 2019, R: A Language and Environment for Statistical Computing: Vienna, Austria, R Foundation for Statistical Computing.

Rivera, T.A., Storey, M., Schmitz, M.D., and Crowley, J.L., 2013, Age intercalibration of $^{40}Ar/^{39}Ar$ sanidine and chemically distinct U/Pb zircon populations from the Alder Creek Rhyolite Quaternary geochronology standard: Chemical Geology, v. 345, p. 87–98, https://doi.org/10.1016/j.chemgeo.2013.02.021.

Roberts, G.O., and Rosenthal, J.S., 2009, Examples of adaptive MCMC: Journal of Computational and Graphical Statistics, v. 18, no. 2, p. 349–367, https://doi.org/10.1198/jcgs.2009.06134.

Sahy, D., Condon, D.J., Terry, D.O., Jr., Fischer, A.U., and Kuiper, K.F., 2015, Synchronizing terrestrial and marine records of environmental change across the Eocene–Oligocene transition: Earth and Planetary Science Letters, v. 427, p. 171–182, https://doi.org/10.1016/j.epsl.2015.06.057.

Schmitz, M.D., and Schoene, B., 2007, Derivation of isotope ratios, errors and error correlations for U-Pb geochronology using ^{205}Pb-^{235}U-(^{233}U)-spiked isotope dilution thermal ionization mass spectrometric data: Geochemistry, Geophysics, Geosystems, v. 8, no. 8, https://doi.org/10.1029/2006GC001492.

Tauber, A.A., 1994, Estratigrafía y vertebrados fósiles de la Formación Santa Cruz (Mioceno inferior) en la costa Atlántica entre las Rías del Coyle y Río Gallegos, Provincia de Santa Cruz, República Argentina [Ph.D. thesis]: Córdoba, Spain, Universidad National de Córdoba, 62 p.

Tauber, A.A., 1997, Bioestratigrafía de la Formación Santa Cruz (Mioceno Inferior) en el extremo sudeste de la Patagonia: Ameghiniana, v. 34, no. 4, p. 413–426.

Tejedor, M.F., Tauber, A.A., Rosenberger, A.L., Swisher, C.C., and Palacios, M.E., 2006, New primate genus from the Miocene of Argentina: Proceedings of the National Academy of Sciences of the United States of America, v. 103, no. 14, p. 5437–5441, https://doi.org/10.1073/pnas.0506126103.

Telford, R.J., Heegaard, E., and Birks, H.J.B., 2004, All age–depth models are wrong: But how badly?: Quaternary Science Reviews, v. 23, no. 1–2, p. 1–5, https://doi.org/10.1016/j.quascirev.2003.11.003.

Vermeesch, P., 2012, On the visualisation of detrital age distributions: Chemical Geology, v. 312, p. 190–194, https://doi.org/10.1016/j.chemgeo.2012.04.021.

Vizcaíno, S.F., Bargo, M.S., Kay, R.F., Fariña, R.A., Di Giacomo, M., Perry, J.M., Prevosti, F.J., Toledo, N., Cassini, G.H., and Fernicola, J.C., 2010, A baseline paleoecological study for the Santa Cruz Formation (late–early Miocene) at the Atlantic coast of Patagonia, Argentina: Palaeogeography, Palaeoclimatology, Palaeoecology, v. 292, no. 3, p. 507–519, https://doi.org/10.1016/j.palaeo.2010.04.022.

Vizcaíno, S.F., Kay, R.F., and Bargo, M.S., 2012a, Background for a paleoecological study of the Santa Cruz Formation (late early Miocene) on the Atlantic coast of Patagonia, *in* Vizcaíno, S.F., Kay, R.F., and Bargo, M.S., eds., Early Miocene Paleobiology in Patagonia: High-Latitude Paleocommunities of the Santa Cruz Formation, p. 1–22, https://doi.org/10.1017/CBO9780511667381.002.

Vizcaíno, S.F., Kay, R.F., and Bargo, M.S., 2012b, Early Miocene Paleobiology in Patagonia: High-Latitude Paleocommunities of the Santa Cruz Formation: Cambridge, UK, Cambridge University Press, https://doi.org/10.1017/CBO9780511667381.

Wetherill, G.W., 1956, Discordant uranium-lead ages: Eos (Washington, D.C.), v. 37, no. 3, p. 320–326.

Wetherill, G.W., 1963, Discordant uranium-lead ages: 2. Discordant ages resulting from diffusion of lead and uranium: Journal of Geophysical Research, v. 68, no. 10, p. 2957–2965, https://doi.org/10.1029/JZ068i010p02957.

Wotzlaw, J.-F., Brack, P., and Storck, J.-C., 2018, High-resolution stratigraphy and zircon U–Pb geochronology of the Middle Triassic Buchenstein Formation (Dolomites, Northern Italy): Precession-forcing of hemipelagic carbonate sedimentation and calibration of the Anisian–Ladinian boundary interval: Journal of the Geological Society, v. 175, no. 1, p. 71–85, https://doi.org/10.1144/jgs2017-052.

Zachos, J., Pagani, M., Sloan, L., Thomas, E., and Billups, K., 2001, Trends, rhythms, and aberrations in global climate 65 Ma to Present: Science, v. 292, no. 5517, p. 686–693, https://doi.org/10.1126/science.1059412.

Science Editor: Bradley S. Singer
Associate Editor: Michael Smith

Manuscript Received 13 December 2018
Revised Manuscript Received 12 March 2019
Manuscript Accepted 23 April 2019

Printed in the USA